

# Physical and Mechanical Behavior of NiTi Composite Fabricated by Newly Developed Uni-Axial Compaction Die

Rajeev Singh<sup>a,c</sup> , Avadesh K Sharma<sup>a\*</sup> , Ajay K Sharma<sup>b</sup> 

<sup>a</sup>Rajkiya Engineering College, Mainpuri-Agra Road, Mainpuri 205119, UP, India

<sup>b</sup>Institute of Engineering and Technology, Sitapur Road, Lucknow 226021, UP, India

<sup>c</sup>Dr. A P J Abdul Kalam Technical University, Lucknow 226031, UP, India

Received: December 02, 2020; Revised: March 23, 2021; Accepted: March 26, 2021

Owing to better mechanical properties and shape memory effect, the NiTi composites fabricated by powder metallurgy are suitable for biomedical implants. However, the excessive porosity and formation of micro-cracks are the major issues related to the NiTi composite. This work focused on developing crack-free dense NiTi composites by newly developed uni-axial compaction die. The work includes the design and manufacturing of uni-axial compaction die. The die was tested by SOLIDWORKS software in a simulated environment. Further, composite samples were successfully fabricated without circumferential micro-cracks at 1910.82 MPa compaction pressure. The effects of compaction pressure on microstructural, densification, and mechanical behavior of NiTi composites were also analyzed. Microstructural characterization shows that the Ni-rich phase increased and the Ti-rich phase decreased with the increase of compaction pressure. The porosity reduces from 17.04 to 8.75% by increasing the compaction pressure from 1273.88 to 1910.82 MPa, and a maximum density of 5.50 g.cm<sup>-3</sup> was obtained. The NiTi<sub>150</sub> composite has similar Young's modulus, and compressive strength (6.93 GPa and 94.36 MPa) compared to cortical and cancellous bone. The high compaction pressure also increases the micro-hardness of NiTi composite up to 453.8 HV<sub>0.5</sub>.

**Keywords:** Composite, compaction, density, strength, hardness.

## 1. Introduction

Nickel-titanium (NiTi) composite with 48–55 Wt.% Ni content is a suitable material for biomedical applications because of their high ductility<sup>1</sup>, good fatigue life<sup>2</sup>, low young's modulus<sup>3,4</sup> and shape memory effect (SME)<sup>5,6</sup>. The mechanical characteristics of the composites depend on their porosity and pores distribution. The porous structure of NiTi composite promotes the development of bone tissues. It also helps to maintain bone-level stiffness to avoid stress shielding and withstand physiological loads for a more extended service life. However, the excessive porosity decreases the mechanical strength of implants<sup>7,8</sup>. Therefore, optimizing the porosity of the composites is essential to achieve suitable mechanical strength and stiffness<sup>9</sup>.

Among several methods, powder metallurgy (PM) is an expeditiously growing technique used to fabricate NiTi composites due to the high melting temperature of Ni and Ti<sup>10</sup>. The composites fabricated by this process show significant mechanical properties due to the uniform dispersion of reinforcement and near-net-shape formability. The PM process minimizes the possibility of microstructural inhomogeneity of fabricated composites<sup>11</sup>. It also prevents or minimizes the requirement of metal removal processes, which considerably reducing manufacturing cost<sup>12</sup>. Chen et al.<sup>13</sup> showed that the manufacturing cost of the Ti parts could be reduced up to 50% for both pure and alloyed Ti. The products prepared using the PM process have controlled characteristics, which

makes this technique more favorable compared to other processes (e.g., forging, extrusion, and casting)<sup>14,15</sup>. A special material or part which is difficult to manufacture by other processes can also be manufactured by the PM process<sup>16-18</sup>. The PM process consists of majorly three steps: mixing different materials, compression, and then heating to bind the particles<sup>19</sup>. According to Qian et al.<sup>20</sup>, the proper compaction of the powder is necessary to form a dense composite with low defects. Several methods are reported (e.g., isostatic compaction and warm compaction) for powder processing, among which uni-axial cold compaction is the easiest method of powder pressing. In this technique, the composite powder is compressed in a compaction die using high pressure in an axial direction<sup>21,22</sup>. After compression, the sample is ejected from the die and sintered at a certain temperature under a controlled condition<sup>23</sup>.

In uni-axial compaction, the compaction pressure lies between 400–600 MPa when high porosity (up to 30%) is required. However, a dense microstructure of NiTi composite can be achieved at high compaction pressure. Several studies show that the compaction pressure directly influences the composite porosity<sup>24,25</sup>. Robertson and Schaffer<sup>12</sup> reported that the NiTi composite was densified with 20% porosity at 1000 MPa, while the dense structure (with 10% porosity) of Ti alloys attained at increased compaction pressure (1800 MPa). One another issue of circumferential micro-cracks appears during uni-axial compaction. These micro-cracks originate due to friction acting between composite particles and the

\*e-mail: sharma.avadesh@gmail.com

die wall during the sample ejection, which can be minimized by providing a suitable arrangement for sample ejection<sup>26-28</sup>. Similarly, the inter-particle friction restricts the repacking and cold working of matrix particles, which also causes micro-cracks during compaction<sup>29</sup>. These micro-cracks can be eliminated at high compaction pressure, which overcomes the inter-particle friction leading to deform the matrix particles<sup>30</sup>.

The present work was aimed to manufacture a new uni-axial compaction die and then successfully fabricate a crack-free dense NiTi composite. The die design was analyzed under a simulated environment by SOLIDWORKS software and experimentally tested by fabricating a NiTi composite. The composite was fabricated by applying a compaction pressure of 1910.82 MPa using a Universal Testing Machine (UTM). Further, the effects of compaction pressure on the physical and mechanical characteristics of the NiTi composite were evaluated. The microstructural characterization of NiTi composites were conducted using Field Emission Scanning Electron Microscopy (FESEM), Energy Dispersive Spectroscopy (EDS), and X-ray Diffraction (XRD). Physical and mechanical characteristics of NiTi composites were examined on the basis of porosity, relative density, compressibility, Young's modulus, compressive strength, and micro-hardness.

## 2. Materials and Methods

### 2.1. Design, fabrication and testing of compaction die

The uni-axial compaction die was fabricated using D3 die steel. D3 is a "D" series die steel that has a high content of carbon (C) and chromium (Cr) (Table 1)<sup>31</sup>. The die steel is a suitable material for die and tooling applications due to excellent wear resistance. The tensile strength, yield strength, and hardness of D3 die steel depends on the condition of heat treatment and lies between 990–2900 MPa, 705–2400 MPa, and 30–69 HRC, respectively<sup>32</sup>. Singh et al.<sup>31</sup> demonstrated that the ultimate compressive strength of D3 steel is equal to 2151 MPa. The yield strength and ultimate compressive strength of heat-treated D3 steel obtained by performing a compression test using 400 kN UTM. The heat-treated D3 steel gives a yield strength of 2153.64 MPa and ultimate compressive strength of 2537.38 MPa. The uni-axial compaction die was designed to fabricate NiTi green compacts with a size of  $\phi 10 \times 15$  mm at 150 kN UTM load. The design calculation of the uni-axial compaction die is given below:

Yield strength,  $\sigma_y = 2150$  MPa (By compression test)

Inner radius of die cylinder,  $R_i = 5$  mm

Outer radius of die cylinder,  $R_o = 45$  mm

Maximum UTM load,  $F = 150$  kN

Cross-section area,  $A = \pi * R_i^2 = 78.5$  mm<sup>2</sup>

Stress developed in the punch at 150 kN UTM load,

$\sigma_1 = F/A = 150000/78.5 = 1910.82$  MPa [ $(\sigma_1 < \sigma_y)$  Hence safe working condition]

Stress developed in the die cylinder due to load on punch,

$\sigma_2 = \sigma_1 \left[ \frac{(R_o)^2 + (R_i)^2}{(R_o)^2 - (R_i)^2} \right] = 1958.59$  MPa [ $(\sigma_2 < \sigma_y)$  Hence safe working condition]

Stress developed in the ejector due to load on punch,

$\sigma_2' = \sigma_1 \left[ \frac{(R_o)^2 + (R_i)^2}{(R_o)^2 - (R_i)^2} \right] = 3184.7$  MPa [ $(\sigma_2' > \sigma_y)$  Die chamber surrounded the ejector which can be absorbed the stress induced in the ejector]

The model of die parts (i.e., die cylinder, punch, stopper, and ejector) was prepared using SOLIDWORKS software (Figure 1a and b). Die material was cut to the required size for die fabrication, and die parts were pre-machined on a CNC lathe machine. After the pre-machining of die parts, three-step heat treatment (stress relieving, hardening, and tempering) was done in the muffle furnace. Stress-relieving was performed at 650 °C for 60 min and die parts were cooled naturally inside the furnace. The die parts were placed in a preheated furnace at 1000 °C for 25–30 min and then quenched in atmospheric air to obtain the suitable hardness. The die parts were again kept in the furnace for tempering, and the temperature was gradually increased to get desired tempering temperature (400 °C). The die parts were cooled naturally inside the furnace. Finally, the die parts were finished using the cylindrical grinder. The finished die cylinder, punch, stopper, and ejector shown in Figure 1c.

The die assembly was analyzed for stress distribution using SOLIDWORKS 2017-18 under simulated conditions. The simulation of die design is based on the von Mises stress criterion. It successfully predicts the failure of material and correctly identifies the failure stress under a one-dimensional tensile or compressive test. The die assembly was analyzed for stress distribution using SOLIDWORKS 2017-18 under simulated conditions. The structural analysis was performed by selecting a round steel element. After selecting the die material (i.e., D3 steel) and giving the required mechanical data, all die parts were assembled and meshed with each other. The bottom surface of the die assembly was considered as a fixed surface and assumed that the 6 g of NiTi powder was poured into the die cavity. Finally, a gradually increased pressure of 1910.82 MPa was applied to the punch. The die performance was also tested by fabricating NiTi composite using 400 kN UTM. After sufficient lubrication, NiTi powder was poured into the die chamber and compacted at 150 kN UTM load (Figure 2a-c).

### 2.2. NiTi composite preparation

Pure Ni and Ti powder having an average particle size of 1036 and 979.5 nm (Figure 3a and b) with 99.99% purity procured from Saveer Biomatrix, India. The average particle size was measured by particle size analyzer (PSA; Malvern Instruments, UK).

The Ni (51 wt.%) and Ti (49 wt.%) powder were mixed and blended in the tumbler ball mill for 6 hours at 100 rpm to get mechanically alloyed NiTi composite powder. The composite mixture was subsequently compacted in compaction die using UTM. To analyze the effects of compaction pressure, composite samples developed at three different compaction pressure (i.e., 1273.88, 1592.35, and 1910.82 MPa) by

**Table 1.** Elemental composition of D3 steel<sup>31</sup>.

Element	C	Cr	Mn	Si	Ni	W	V	P	S	Cu
<b>Content (%)</b>	2.1	12	0.6	0.6	0.3	1	1	0.03	0.03	0.25

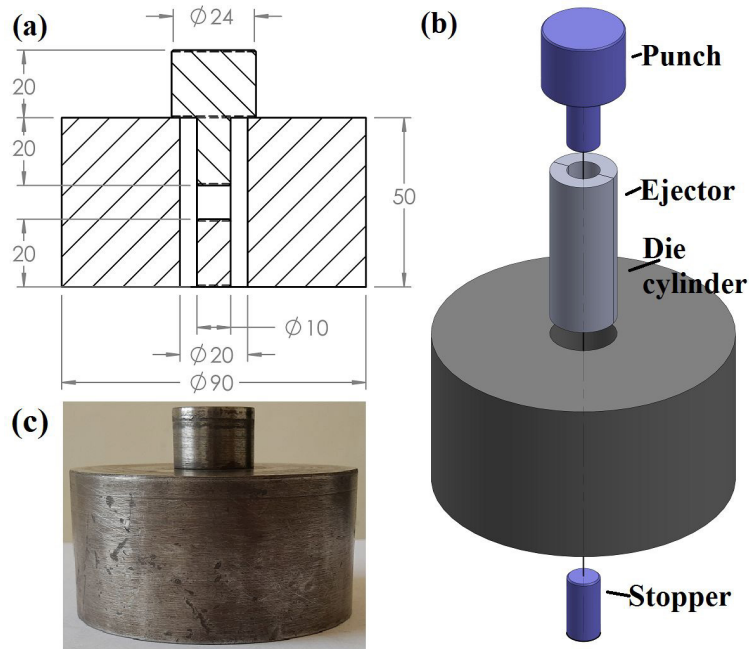


**Figure 1.** (a) 2D model of compaction die with dimensions (all dimensions in mm), (b) various die parts and (c) finished die assembly with punch, stopper and ejector.



**Figure 2.** (a) Uni-axial compaction of NiTi composite powder on UTM, (b) enlarged view of white square showing die arrangement and (c) enlarged view of black square showing displacement of punch with UTM load.

applying the load of 100, 125, and 150 kN using UTM (Figure 4a). The composites were named NiTi<sub>100</sub>, NiTi<sub>125</sub>, and NiTi<sub>150</sub> based on the load applied using UTM. The NiTi compacts were sintered in a vacuum furnace at 950 °C for 6 hours using a 20 °C/min heating rate. Two additional pauses of 15 min were given at 300 °C and 600 °C to minimize cracks' formation due to differences in thermal coefficients of metals. Finally, sintered samples (Figure 4b) cooled naturally inside the furnace.

### 2.3. Microstructural characterization

The morphology and elemental details of raw Ni and Ti powder were investigated by FESEM (FEI FESEM Quanta FEG 200, Netherland) and attached EDS (X-Max 50, Oxford Instruments, UK). For microscopic analysis, the cross-sectional surface of the sintered samples polished up to 2500 grit silicon carbide (SiC) abrasive paper followed by fine lapping with 0.5  $\mu$ m alumina (Al<sub>2</sub>O<sub>3</sub>) suspension and etching with etchant no. 151 (ASTM 407–7<sup>e1</sup>).

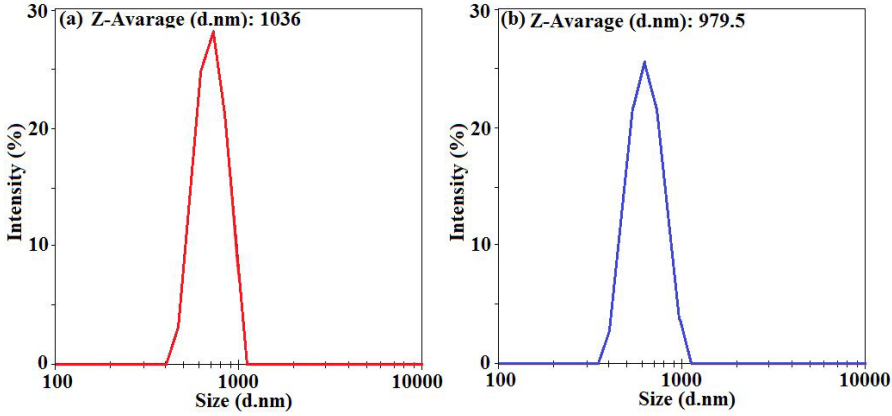


**Figure 3.** Average particle size with particle distribution of (a) Ni and (b) Ti powder measured by particle size analyzer (PSA; Malvern instruments, UK).



**Figure 4.** (a) NiTi composite samples after compaction at 1273.88, 1592.35 and 1910.82 MPa compaction pressure with sample id NiTi<sub>100</sub>, NiTi<sub>125</sub> and NiTi<sub>150</sub> respectively, (b) NiTi composite samples after sintering, (c) composite sample developed with ejector has no cracks on its circumference and (d) composite sample developed without ejector shows several cracks.

Finally, the samples were washed with alcohol and dried in atmospheric air. The microstructure and pore characteristics of sintered samples were evaluated by FESEM (FEI NOVA NANO FESEM 450, Netherland) at an accelerated voltage of 15 kV. The developed phases of NiTi composites were examined by XRD (Panalytical X'pert powder pro, Malvern, UK). The XRD patterns were obtained using Cu K $\alpha$  radiation, up to 30<sup>o</sup>–80<sup>o</sup> scanning range with a scan step size of 0.03<sup>o</sup>.

#### 2.4. Density and compressibility behavior

The theoretical density of composite samples was calculated using the mixing rule given in Equation 1.

$$\rho_{th} = 1 / \left\{ \left( \frac{wt_{Ni}}{\rho_{Ni}} \right) + \left( \frac{wt_{Ti}}{\rho_{Ti}} \right) \right\} \quad (1)$$

where  $\rho_{th}$  is theoretical density,  $wt_{Ni}$  and  $wt_{Ti}$  are weight proportion of matrix materials, and  $\rho_{Ni}$  and  $\rho_{Ti}$  are the density of matrix materials. The sintered density of composite samples was measured using the Archimedes principle. The relative density and porosity of sintered composites were calculated using Equations 2 and 3.

$$\rho_r = \left( \rho_{sinter} / \rho_{th} \right) \times 100 \quad (2)$$

$$p = \left\{ 1 - \left( \rho_{sinter} / \rho_{th} \right) \right\} \times 100 \quad (3)$$

where  $\rho_r$  is relative density,  $p$  is porosity, and  $\rho_{sinter}$  is the density of composites after sintering. Further, the porosity was also analyzed by ImageJ software. The interconnected porosity of the composites was evaluated by a water absorption test. The composite samples were weighed in electronic balance before immersion and after six days of immersion in deionized water. Finally, the water absorption was calculated by Equation 4.

$$W_{abs} = \left\{ \left( m_f - m_i \right) / m_i \right\} \times 100 \quad (4)$$

where  $W_{abs}$  is water absorption in wt.%,  $m_f$  is the final mass of the composite sample after immersion, and  $m_i$  initial mass of the composite sample. The % water absorption represents the interconnected porosity of NiTi composites.

Parilak et al.<sup>21</sup> reported many compaction equations to analyze the compressibility behavior of the metal powders, in which Heckel's equation<sup>33</sup> (Equation 5) was used to investigate the compressibility behavior of NiTi composites. The equation is based on the linear regression between the compaction pressure and the relative density.

$$\ln \left\{ 1 / (1 - \rho_r) \right\} = K_1 P + A_1 \quad (5)$$

where  $P$  is the compaction pressure (MPa),  $K_1$  is a constant that denotes the powder's compressibility, and  $A_1$  is the y-intercept.

## 2.5. Mechanical properties

The mechanical characteristics of NiTi composites were evaluated by identifying Young's modulus and ultimate compressive strength of sintered composites. The compression test was carried out according to a standard compressive testing method for metallic materials (ISO 13314) at room temperature. A square shape sample with 8.5 mm thickness and 13 mm length was used for the compression test. The test was performed using UTM (Instron-5967) with a 0.25 kN/min load rate. The micro-hardness of the composites identified using a Vickers hardness tester (Innovatest). The micro-hardness was measured with the average value of 5 measurements on each sample at a load of 0.5 kg with 10 second dwell time.

## 3. Results and Discussion

### 3.1. Testing of compaction die

The die assembly was analyzed for stress distribution using SOLIDWORKS 2017-18 under simulated conditions. It is found that the stress distributed along to the direction of load, and no deformation was observed in the die parts (Figure 5). The die cylinder has minimum stress of 8.896 MPa, and the stopper and compact have maximum stress of 2038 MPa. The compaction was performed at gradually increased load. At 150 kN compaction load, the maximum stress developed in the die parts (i.e., stopper and compact) is lower than the

yield strength ( $\sigma_y$ ) of the die material and remains in safe working range (i.e., i.e., 2038 MPa < 2150 MPa). That is why the compaction of the samples was completed without affecting the compaction die.

The compaction die was analyzed experimentally by fabricating a NiTi green compact at 1910.82 MPa compaction pressure. The green compacts were successfully fabricated without any considerable deformation in the compaction die. It is observed that the composite samples do not have any circumferential cracks. However, the sample compacted without an ejector shows several cracks (Figure 4c). These cracks were eliminated due to high compaction pressure and incorporation of an ejector. The high compaction pressure minimizes the inter-particle friction, and the ejector eliminates the friction between the die wall and composite particles during sample ejection. The ejector was placed in the die chamber and samples were compressed in the ejector. After successful compaction, the ejector was removed from the die chamber and separated into two equal parts perpendicular to the direction of load. Finally, the composite compacts were easily removed without using any axial force.

### 3.2. Microstructural characterization

The FESEM images of raw Ni and Ti powder are shown in Figure 6a and b. It is observed that Ni reveals a spherical shape while Ti possesses flake-like spongy morphology. The EDS spectrum showed higher peaks for Ni and Ti that confirms the purity of these powders. However, some

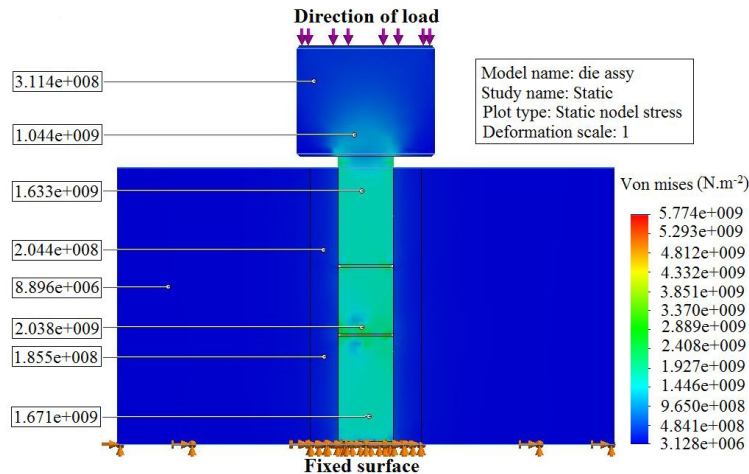


Figure 5. Stress distribution (von Mises) on uni-axial compaction die and compacted powder under simulated conditions.

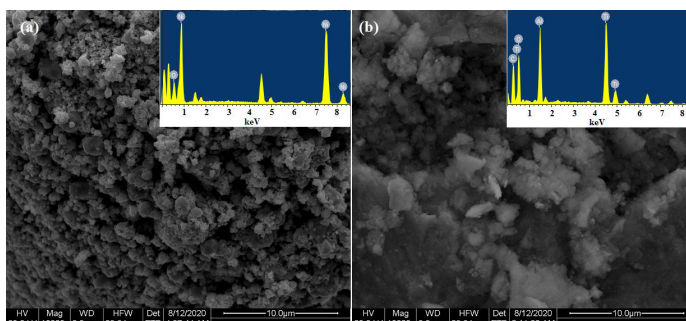


Figure 6. FESEM images of as received (a) Ni and (b) Ti powder with their EDS spectrum.

impurities such as aluminium (Al) and carbon (C) were observed in a negligible amount.

Figure 7a-c shows FESEM micrographs of NiTi composites developed at different compaction pressure. The micrographs reveal the phase distribution in which NiTi and other phases such as NiTi<sub>2</sub> and Ni<sub>3</sub>Ti were identified based on contrast. To quantify the developed phases, these micrographs were also processed by ImageJ software (Figure 7d). The analysis shows that the NiTi<sub>100</sub> composite has 39.52% area fraction of NiTi<sub>2</sub>, 8.52% area fraction of Ni<sub>3</sub>Ti, and 32.72% area fraction of NiTi phases, while NiTi<sub>125</sub> has 32.24% of NiTi<sub>2</sub>, 16.66% Ni<sub>3</sub>Ti, and 37.93% NiTi phases. The NiTi<sub>150</sub> composite showed an increase of NiTi and Ni<sub>3</sub>Ti phases (41.12% and 21.25%) and decrease of NiTi<sub>2</sub> phase (27.86%). These phases are formed due to the lower Gibbs free energy compared to NiTi at the sintering temperature of 950 °C. The results show that the Ni-rich phases increased, and the Ti-rich phase decreased with the increase of compaction pressure from 1273.88 to 1910.82 MPa. It is found that the porosity decreases at an elevated compaction pressure, promoting the diffusion mechanism, and Ni diffuses faster than Ti. A dense structure of composite promotes inter-particle heat transfer. On the other side, the composite compacted at low compaction pressure restricts the flame propagation and causes incomplete synthesis due to excessive porosity<sup>34</sup>. Zhou et al.<sup>35</sup> prepared two-layer NiTi alloy with 52% and 14% porosity through a cold compaction process. Both layers have B2 NiTi as a major phase and some secondary phases such as NiTi<sub>2</sub>, Ni<sub>3</sub>Ti, and Ni<sub>4</sub>Ti<sub>3</sub>. The inner layer with 52% porosity has more secondary phases compared to the dense outer layer (with 14% porosity). Zhang et al.<sup>36</sup> reported a single NiTi

phase and some secondary phases (e.g., NiTi<sub>2</sub> and Ni<sub>3</sub>Ti) formed with a dense structure (18% porosity). However, the excessive porosity (61%) causes large secondary phases due to improper sintering. These secondary phases formed because of the slow diffusion of atoms, which reveals that sample porosity strongly influences the sintering characteristics. The concentration of these phases also relies on the sintering temperature and aging time. Wang and Hu<sup>37</sup> demonstrated that the secondary Ni<sub>3</sub>Ti and NiTi<sub>2</sub> phases decreased and the NiTi phase increased at longer sintering time (approx. 6 hours). High sintering temperature (900 to 1000 °C) also promotes the transformation of these secondary phases into the primary NiTi phase.

Figure 8 shows the XRD pattern of the ball-milled NiTi powder and sintered NiTi<sub>150</sub> composite. The peaks of the NiTi<sub>0.921</sub> phase were observed in the XRD pattern of ball-milled NiTi composite powder which confirmed the mechanical alloying of Ni with Ti. However, some peaks of unalloyed Ni were also observed. The XRD pattern of sintered NiTi<sub>150</sub> composite consists of desirable B19' (martensite NiTi) and B2 (austenite NiTi) with some other phases (i.e., Ni<sub>3</sub>Ti and NiTi<sub>2</sub>). The closely packed Ni and Ti particles at high compaction pressure accelerate the alloying of the NiTi and promote NiTi phase formation due to enhanced diffusion of atoms<sup>38,39</sup>.

### 3.3. Density and compressibility behavior

The theoretical density of NiTi composite was calculated by the mixing rule given in Equation 1. The sintered density of NiTi composites was obtained by the Archimedes principle. Table 2 reveals that the density of composite

**Table 2.** Theoretical density, sintered density, relative density and porosity of NiTi composites developed at different compaction pressure.

Samples	Th. Density ( $\rho_{th}$ )(g.cm <sup>-3</sup> )	Sintered density ( $\rho_{sinter}$ ) (g.cm <sup>-3</sup> )	Relative density ( $\rho_r$ ) (%)	Porosity (p) (%)
NiTi <sub>100</sub>	6.027	5.00	82.96	17.04
NiTi <sub>125</sub>	6.027	5.22	86.61	13.39
NiTi <sub>150</sub>	6.027	5.50	91.25	8.75

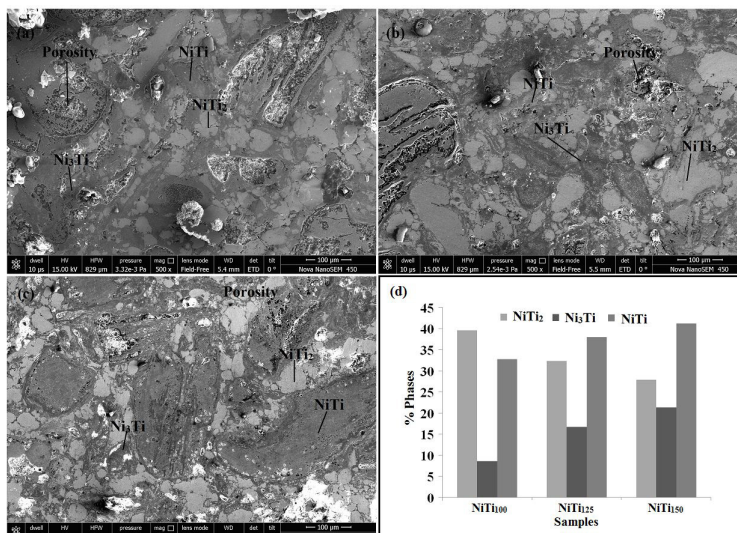


**Figure 7.** FESEM micrographs of (a) NiTi<sub>100</sub>, (b) NiTi<sub>125</sub>, (c) NiTi<sub>150</sub> composites showing microstructure and developed phases and (d) quantification of developed phases processed by ImageJ software.

samples increased from 5.00 to 5.50 g.cm<sup>-3</sup> with an increase of compaction pressure from 1273.88 to 1910.82 MPa. Further, the porosity of NiTi composites was calculated by the formula given in Equation 3. The results show that the porosity decreased from 17.04 to 8.75% due to adequate bonding and homogeneous dispersion of matrix elements at elevated compaction pressure. The NiTi<sub>100</sub> composite shows larger pores with significant interconnectivity, while the NiTi<sub>125</sub> and NiTi<sub>150</sub> composites show dense structures with 13.39 and 8.75% porosity (Figure 7a-c).

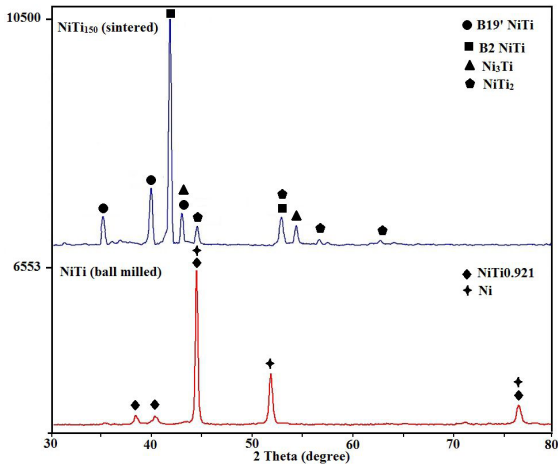


**Figure 8.** XRD patterns of NiTi composite powder after ball milling and sintered NiTi<sub>150</sub> composite.

The porosity of composites was also analyzed by ImageJ software (Figure 9a-d). The red color shows the area fraction of pores formed on NiTi composites' surface. It reveals that the pore area was reduced from 19.27 to 9.62% by increasing the compaction pressure from 1273.88 to 1910.82 MPa. The porosity identified by ImageJ software is similar to porosity determined by the Archimedes principle. Table 3 indicates the water absorption of NiTi composites developed at different compaction pressure. The NiTi<sub>100</sub>, NiTi<sub>125</sub>, and NiTi<sub>150</sub> composites show the water absorption of 3.52, 3.11, and 2.62%, respectively. The % water absorption indicates the amount of interconnected porosity which was reduced at elevated compaction pressure.

The densification behavior of NiTi powder is analyzed through displacement versus load curve shown in Figure 10a. The compaction pressure directly influences the densification behavior of NiTi; i.e., relative density increases with the increase of compaction pressure (Table 2). By increasing the compaction pressure from 0 to 1273.88 MPa, rapid powder compaction was observed, and the relative density reached up to 82.96%. At 1592.35 MPa compaction pressure, gradually increased relative density (86.61%) was achieved. A maximum relative density of 91.25% was obtained at the highest compaction pressure of 1910.82 MPa. It is observed that the increased compaction pressure promotes the densification of NiTi composite due to enhanced bonding between matrix materials. Khoei et al.<sup>40</sup> reported the three stages of powder densification during uni-axial compaction. In the initial step (stage 1) of densification, the composite powders form in

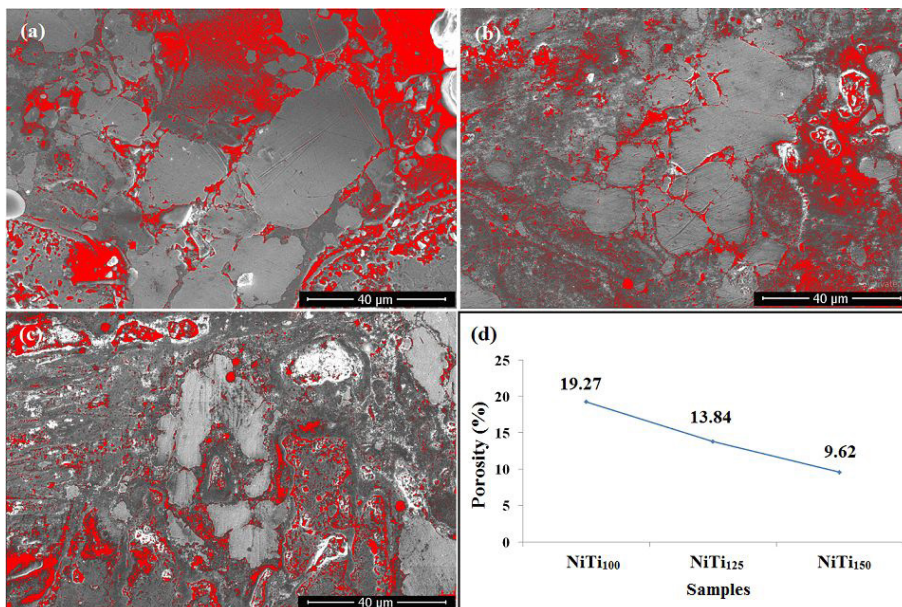


**Figure 9.** FESEM micrographs of (a) NiTi<sub>100</sub>, (b) NiTi<sub>125</sub>, (c) NiTi<sub>150</sub> composites showing pore distribution and (d) quantification of porosity processed by ImageJ software.

**Table 3.** Water absorption showing the interconnected porosity of NiTi composites identified by water absorption test.

Samples	Initial mass ( $m_i$ ) (g)	Final mass ( $m_f$ ) (g)	Water absorption ( $W_{abs}$ ) (%)
NiTi <sub>100</sub>	5.68	5.88	3.52
NiTi <sub>125</sub>	5.77	5.95	3.11
NiTi <sub>150</sub>	5.72	5.87	2.62

the transitional repositioning in which the powder particles are moved to each other and repacked under compaction pressure. After particle repacking, the inter-particle motion decreases, and the particles start to deform elastically. At this stage, the relative density of composite powder increases rapidly under the low compaction pressure. In stage 2, plastic deformation occurs at the particle's contact area which leads to particle interlocking due to the dislocations developed from the composite particles. Densification of the powder after these two stages is known as geometric hardening. In the last step (Stage 3), when no space is available for inter-particle motion, plastic deformation occurs inside the individual particles, and densification occurs due to the cold working of composite particles. The particles offer high resistance to deformation at this stage, and increased pressure is required to complete the compaction<sup>41</sup>.

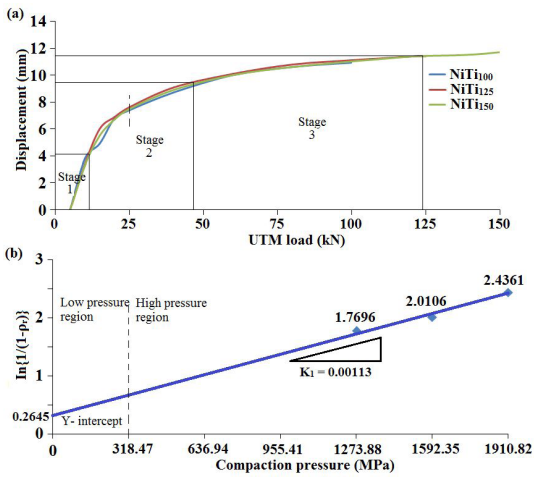


**Figure 10.** (a) Displacement versus load (UTM) curve showing densification behaviour of NiTi composites developed at different compaction pressure and (b) compressibility curve on the basis of Heckel equation.

Figure 10b demonstrated the compressibility analysis of NiTi powder using the Heckel compaction equation. The analysis shows that the NiTi powder has low compressibility in the high-pressure region (i.e.,  $K_1 = 0.00113$  for  $P \geq 1273.88$  MPa). The density of Ni is two times higher than the density of Ti, which restricts the plastic deformation of NiTi powder at high compaction pressure and minimizes the compressibility of NiTi powder. It is observed that the linear plot of compressibility behavior (Figure 10b) does not follow the experimental data of Figure 10a at a low compaction pressure. Hadadzadeh et al.<sup>42</sup> reveal that the Ti powder's compressibility in the low-pressure area ( $K_1 = 0.0064$ ) was approx. two times greater than the compressibility in the high-pressure region ( $K_1 = 0.0031$ ). To analyze the compressibility of NiTi powder in more detail, the data divided into low-pressure (<318.47 MPa) and high-pressure region (>318.47 MPa). In the low-pressure region, the composite's relative density increases quickly, and the densification occurs due to void collapse and particle interlocking. In the high-pressure region, the composite particles deform plastically and exhibited high resistance to densification due to strain hardening of the particles. Therefore, the relative density of powder increases very slowly and eventually becomes constant.

### 3.4. Mechanical properties

Young's modulus, ultimate compressive strength, and micro-hardness of NiTi composites are shown in Table 4. It reveals that the increase of compaction pressure positively affects the mechanical characteristics of the NiTi composite. Figure 11a shows the compressive stress-strain curves of NiTi composites fabricated at different compaction pressure. The compressive strength of the NiTi composite increased from 57.21 to 94.36 MPa due to increased compaction pressure from 1273.88 to 1910.82 MPa. The NiTi<sub>125</sub> composite offers a higher load capacity compared to the NiTi<sub>100</sub> composite. The high porosity remains at low compaction pressure. So when the stress reached at the end of plastic deformation, several pores collapsed layer by layer and cause a sharp

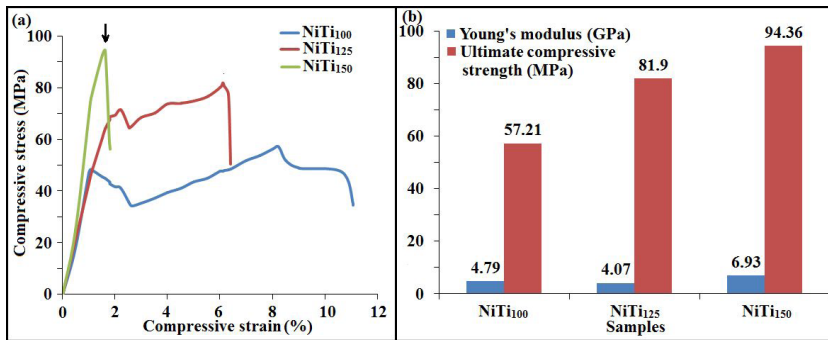


**Figure 11.** (a) Compressive stress-strain curve of NiTi composites developed at different compaction pressure and (b) Young's modulus and ultimate compressive strength of NiTi<sub>100</sub>, NiTi<sub>125</sub> and NiTi<sub>150</sub> composites.

**Table 4.** Young's modulus, ultimate compressive strength and micro-hardness of NiTi composites developed at different compaction pressure.

Samples	Young's modulus (GPa)	Ultimate compressive strength (MPa)	Microhardness (HV <sub>0.5</sub> )
NiTi <sub>100</sub>	4.79	57.21	239.5
NiTi <sub>125</sub>	4.07	81.9	350.6
NiTi <sub>150</sub>	6.93	94.36	453.8

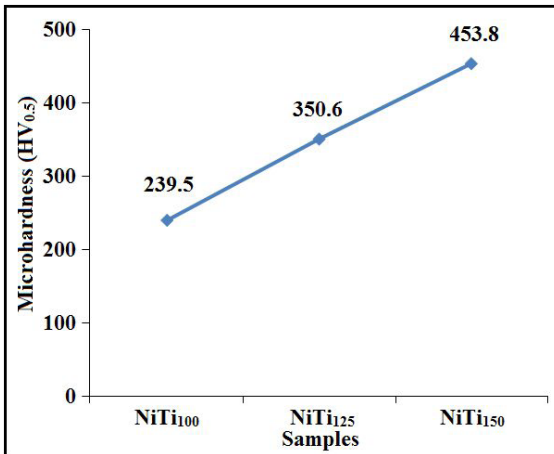


**Figure 12.** Micro-hardness (HV<sub>0.5</sub>) of NiTi<sub>100</sub>, NiTi<sub>125</sub> and NiTi<sub>150</sub> composites.

reduction of stress<sup>43</sup>. Similarly, the large interconnected pores and weak interfacial bonds resist the stress transfer and reduce compressive strength. The result shows that the NiTi<sub>150</sub> composite has the highest compressive strength (94.36 MPa), but it exhibits an early failure behavior (as marked by arrows in Figure 11a). At high compaction pressure, the composite is densified by the cold working of particles which restricts its plastic deformation, and eventually, early failure occurred during the compression test.

Figure 11b shows that Young's modulus and compressive strength of the NiTi composites increase with elevated compaction pressure. The Young's modulus and ultimate compressive strength of NiTi<sub>100</sub> composite reached up to 4.79 GPa and 57.21 MPa, respectively. At 1592.35 MPa compaction pressure, the compressive strength increased to 81.9 MPa, and Young's modulus slightly decreased to 4.07 GPa. By increasing the compaction pressure up to 1910.82 MPa, the highest Young's modulus and compressive strength were achieved. The NiTi<sub>150</sub> composite shows the highest compressive strength of 94.36 MPa which is similar and higher than the compressive strength of human bones (15–35 and 49–148 MPa for cancellous and cortical bones, respectively<sup>44</sup>). Similarly, Young's modulus of the NiTi composites fabricated by uni-axial compaction (4.07 to 6.93 GPa) significantly match Young's modulus of human bones (0.05–0.5 and 3–20 GPa for cancellous and cortical bones, respectively<sup>45</sup>).

It is observed that the micro-hardness of the NiTi composites increases with the increase of compaction pressure. The NiTi<sub>125</sub> composite shows increased micro-hardness (350.6 HV<sub>0.5</sub>) compared to the hardness of the NiTi<sub>100</sub> composite (239.5 HV<sub>0.5</sub>). The highest hardness (453.8 HV<sub>0.5</sub>) was identified for the NiTi<sub>150</sub> composite, as shown in Table 4. The highest hardness for this composite is obtained due to the increased compaction pressure, which provides a highly dense structure with strong bonding between powder particles<sup>46</sup>. Similarly, the hardness of composite is also influenced by the increase of Ni<sub>3</sub>Ti phase and decrease of NiTi<sub>2</sub> phase (Figure 7d). The micro-hardness increased up to 453.8 HV<sub>0.5</sub>, which showed a sharp rise of 89.47% for NiTi<sub>150</sub> composite compared to NiTi<sub>100</sub> composite (Figure 12)

due to closely packed microstructure and the presence of large Ni<sub>3</sub>Ti phase<sup>47</sup>.

#### 4. Conclusions

The new uni-axial compaction die was designed and manufactured to develop NiTi composite at high compaction pressure. The NiTi composite was successfully synthesized by the newly developed compaction die without any considerable cracks. The results show that the compaction pressure has a significant effect on the physical and mechanical properties of NiTi composite. Microstructural analysis reveals the homogenous dispersion of NiTi phases. In contrast, the quantification of phases shows that NiTi and Ni<sub>3</sub>Ti phases increased, and NiTi<sub>2</sub> phase decreased with the increase of compaction pressure. The reduced porosity (17.04 to 8.75%) and interconnected pores (3.52 to 2.62%) were identified by increasing the compaction pressure from 1273.88 to 1910.82 MPa. A dense structure of NiTi composite was obtained with 5.50 g.cm<sup>-3</sup> sintered density at 1910.82 MPa compaction pressure. Three-stage densification behavior was analyzed, which shows an elastic, plastic, and cold working stage of NiTi composite. However, low compressibility was identified due to the presence of high Ni content, which restricts the plastic deformation of composite particles. It is found that the mechanical properties such as Young's modulus and ultimate compressive strength increased from 4.07 to 6.93 GPa and 57.21 to 94.36 MPa, respectively, due to increased compaction pressure from 1273.88 to 1910.82 MPa. The micro-hardness of composites increased up to 89.47%, and the NiTi<sub>150</sub> composite exhibited the highest value of 453.8 HV<sub>0.5</sub>. Similarly, the composite (NiTi<sub>150</sub>) developed at 1910.82 MPa compaction pressure reveals dense microstructure with similar Young's modulus and compressive strength compared to the human bone which makes it suitable for biomedical implants.

#### 5. Acknowledgements

The author, Rajeev Singh is grateful to Dr A P J Abdul Kalam Technical University, Lucknow, India for providing PhD assistantship (AKTU/Dean-PGSR/PhD/2019/5847) under the Homi Bhabha teaching fellowship scheme.

#### 6. References

- Elahinia M, Shayesteh Moghaddam N, Taheri Andani M, Amerinatanzi A, Bimber BA, Hamilton RF. Fabrication of NiTi through additive manufacturing: a review. *Prog Mater Sci.* 2016;83:630-63.
- Bagheri A, Mahtabi MJ, Shamsaei N. Fatigue behavior and cyclic deformation of additive manufactured NiTi. *J Mater Process Technol.* 2018;252:440-53.
- Rony L, Lancigu R, Hubert L. Intraosseous metal implants in orthopedics: a review. *Morphologie.* 2018;110(339):231-42.
- Cluff D, Corbin SF. The influence of Ni powder size, compact composition and sintering profile on the shape memory transformation and tensile behaviour of NiTi. *Intermetallics.* 2010;18(8):1480-90.
- Sabahi N, Chen W, Wang C-H, Kruzic JJ, Li X. A review on additive manufacturing of shape-memory materials for biomedical applications. *JOM.* 2020;72:1229-53.
- Saedi S, Saghaian SE, Jahadakar A, Shayesteh Moghaddam N, Taheri Andani M, Saghaian SM, et al. Shape memory response of porous NiTi shape memory alloys fabricated by selective laser melting. *J Mater Sci Mater Med.* 2018;29:40.

7. Zhang L, He ZY, Tan J, Zhang YQ, Stoica M, Calin M, et al. Designing a novel functional-structural NiTi/hydroxyapatite composite with enhanced mechanical properties and high bioactivity. *Intermetallics*. 2017;84:35-41.
8. Xu JL, Bao LZ, Liu AH, Jin XJ, Tong YX, Luo JM, et al. Microstructure, mechanical properties and superelasticity of biomedical porous NiTi alloy prepared by microwave sintering. *Mater Sci Eng C*. 2015;46:387-93.
9. Tosun G, Ozler L, Kaya M, Orhan N. A study on microstructure and porosity of NiTi alloy implants produced by SHS. *J Alloys Compd*. 2009;487(1-2):605-11.
10. Kaya M, Çakmak Ö, Gülenç B, Atlı KC. Thermomechanical cyclic stability of porous NiTi shape memory alloy. *Mater Res Bull*. 2017;95:243-7.
11. Farvizi M, Javan MK, Akbarpour MR, Kim HS. Fabrication of NiTi and NiTi-nano Al<sub>2</sub>O<sub>3</sub> composites by powder metallurgy methods: comparison of hot isostatic pressing and spark plasma sintering techniques. *Ceram Int*. 2018;44(13):15981-8.
12. Robertson IM, Schaffer GB. Review of densification of titanium based powder systems in press and sinter processing. *Powder Metall*. 2010;53(2):146-62.
13. Chen W, Yamamoto Y, Peter WH, Gorti SB, Sabau AS, Clark MB, et al. Cold compaction study of Armstrong Process® Ti-6Al-4V powders. *Powder Technol*. 2011;214(2):194-9.
14. Bolzoni L, Yang F. Development of Cu-bearing powder metallurgy Ti alloys for biomedical applications. *J Mech Behav Biomed Mater*. 2019;97:41-8.
15. Pokorska I. Deformation of powder metallurgy materials in cold and hot forming. *J Mater Process Technol*. 2008;196(1-3):15-32.
16. Guo W, Liu B, Liu Y, Li T, Fu A, Fang Q, et al. Microstructures and mechanical properties of ductile NbTaTiV refractory high entropy alloy prepared by powder metallurgy. *J Alloys Compd*. 2019;776:428-36.
17. Luo SD, Song T, Lu SL, Liu B, Tian J, Qian M. High oxygen-content titanium and titanium alloys made from powder. *J Alloys Compd*. 2020;836:155526.
18. Kulkarni H, Dabhade VV. Green machining of powder-metallurgy-steels (PMS): an overview. *J Manuf Process*. 2020;44:1-18.
19. Suryanarayana C, Al-Aqeeli N. Mechanically alloyed nanocomposites. *Prog Mater Sci*. 2013;58(4):383-502.
20. Qian M, Yang YF, Yan M, Luo SD. Design of low cost high performance powder metallurgy titanium alloys: some basic considerations. *Key Eng Mater*. 2012;520:24-9.
21. Parilak L, Dudrova E, Bidulsky R, Kabatova M. Derivation, testing and application of a practical compaction equation for cold die-compacted metal powders. *Powder Technol*. 2017;322:447-60.
22. Jabur AS, Al-Haidary JT, Al-Hasani ES. Characterization of Ni-Ti shape memory alloys prepared by powder metallurgy. *J Alloys Compd*. 2013;578:136-42.
23. Guo R, Liu B, Xu R, Cao Y, Qiu J, Chen F, et al. Microstructure and mechanical properties of powder metallurgy high temperature titanium alloy with high Si content. *Mater Sci Eng A*. 2020;777:138993.
24. Tay BY, Goh CW, Gu YW, Lim CS, Yong MS, Ho MK, et al. Porous NiTi fabricated by self-propagating high-temperature synthesis of elemental powders. *J Mater Process Technol*. 2008;202(1-3):359-64.
25. Gased NM, Al-Ethari HA, Haleem AH. Effect of compacting pressure on microstructure, physical and mechanical properties of NiTi SMA. *Al-Qadisiyah J Eng Sci*. 2018;9:171-82.
26. Leon CA, Rodriguez-Ortiz G, Aguilar-Reyes EA. Cold compaction of metal-ceramic powders in the preparation of copper base hybrid materials. *Mater Sci Eng A*. 2009;526(1-2):106-12.
27. Zhou J, Zhu C, Zhang W, Ai W, Zhang X, Liu K. Experimental and 3D MPFEM simulation study on the green density of Ti-6Al-4V powder compact during uniaxial high velocity compaction. *J Alloys Compd*. 2020;817:153226.
28. Arifin A, Sulong AB, Muhamad N, Syarif J, Ramli MI. Material processing of hydroxyapatite and titanium alloy (HA/Ti) composite as implant materials using powder metallurgy: a review. *Mater Des*. 2014;55:165-75.
29. Al-Qureshi HA, Soares MRF, Hotza D, Alves MC, Klein AN. Analyses of the fundamental parameters of cold die compaction of powder metallurgy. *J Mater Process Technol*. 2008;199(1-3):417-24.
30. Rolland SA, Mosbah P, Gethin DT, Lewis RW. Lode dependency in the cold die powder compaction process. *Powder Technol*. 2012;221:123-36.
31. Singh RB, Seema, Kumar D. Heat treatment of tool steel D3 and effects on mechanical properties. *Int J Recent Sci Res*. 2019;10(5):32540-5.
32. Ghazi SS, Mashloosh KM. Influence of heat treatment on resistance of wear and mechanical properties of die steel kind D3. *Am J Sci Ind Res*. 2015;5(2):33-40.
33. Heckel RW. Density-pressure relationships in powder compaction. *Trans Metall Soc AIME*. 1961;221:671-5.
34. Yeh C, Sung W. Synthesis of NiTi intermetallics by self-propagating combustion. *J Alloys Compd*. 2004;376(1-2):79-88.
35. Zhou D, Gao Y, Lai M, Li H, Yuan B, Zhu M. Fabrication of NiTi shape memory alloys with graded porosity to imitate human long-bone structure. *J Bionics Eng*. 2015;12(4):575-82.
36. Zhang L, Zhang YQ, Jiang YH, Zhou R. Superelastic behaviors of biomedical porous NiTi alloy with high porosity and large pore size prepared by spark plasma sintering. *J Alloys Compd*. 2015;644:513-22.
37. Wang J, Hu K. Phase transformation of NiTi alloys during vacuum sintering. *IOP Conf Series Mater Sci Eng*. 2017;204:012023.
38. Wang X, Yu J, Liu J, Chen L, Yang Q, Wei H, et al. Effect of process parameters on the phase transformation behavior and tensile properties of NiTi shape memory alloys fabricated by selective laser melting. *Addit Manuf*. 2020;36:101545.
39. Novák P, Moravec H, Salvetr P, Průša F, Drahoukoupil J, Kopeček J, et al. Preparation of nitinol by non-conventional powder metallurgy techniques. *Mater Sci Technol*. 2015;31(15):1886-93.
40. Khoei AR, Sameti AR, Mofatteh H. Compaction simulation of crystalline nano-powders under cold compaction process with molecular dynamics analysis. *Powder Technol*. 2020;373:741-53.
41. Cristofolini I, Molinari A, Pederzini G, Rambelli A. Study of the uniaxial cold compaction of AISI 316L stainless steel powders through single action tests. *Powder Technol*. 2016;295:284-95.
42. Hadadzadeh A, Whitney MA, Wells MA, Corbin SF. Analysis of compressibility behavior and development of a plastic yield model for uniaxial die compaction of sponge titanium powder. *J Mater Process Technol*. 2017;243:92-9.
43. Parvizi S, Hasannaemi V, Saebnoori E, Shahrazi T, Sadrnezhad SK. Fabrication of porous NiTi alloy via powder metallurgy and its mechanical characterization by shear punch method. *Russ J Non-Ferrous Met*. 2012;53(2):169-75.
44. Abidi IH, Khalid FA, Farooq MU, Hussain MA, Maqbool A. Tailoring the pore morphology of porous nitinol with suitable mechanical properties for biomedical applications. *Mater Lett*. 2015;154:17-20.
45. Geetha M, Singh AK, Asokamani R, Gogia AK. Ti based biomaterials, the ultimate choice for orthopedic implants-A review. *Prog Mater Sci*. 2009;54(3):397-425.
46. Khanlari K, Ramezani M, Hayat M, Piaras K, Cao P, Neitzert T. Microstructural and mechanical properties of porous 60NiTi prepared by conventional press-and-sinter method. *MATEC Web Conf*. 2017;109:01002.
47. Akmal M, Raza A, Khan MM, Khan MI, Hussain MA. Effect of nano-hydroxyapatite reinforcement in mechanically alloyed NiTi composites for biomedical implant. *Mater Sci Eng C*. 2016;68:30-6.